

Communication

Physicochemical Properties of Yttria-Stabilized-Zirconia In-Flight Particles during Supersonic Atmospheric Plasma Spray

Guozheng Ma ¹, Pengfei He ¹, Shuying Chen ^{2,*}, Jiajie Kang ^{3,*} , Haidou Wang ¹, Ming Liu ¹, Qin Zhao ^{1,4} and GuoLu Li ⁴

¹ National Key Lab for Remanufacturing, Army Academy of Armored Forces, Beijing 100072, China

² National Key Laboratory of Human Factors Engineering, China Astronaut Research and Training Center, Beijing 100094, China

³ School of Engineering and Technology, China University of Geosciences, Beijing 100083, China

⁴ School of Materials Science and Engineering, Hebei University of Technology, Tianjin 300130, China

* Correspondence: chenshuying90@163.com (S.C.); kangjiajie@cugb.edu.cn (J.K.); Tel.: +86 10 66718475 (S.C.); Fax: +86 10 66717144 (S.C.)

Received: 12 May 2019; Accepted: 27 June 2019; Published: 8 July 2019



Abstract: In order to achieve better knowledge of the thermal barrier coatings (TBCs) by supersonic atmospheric plasma spraying (SAPS) process, an experimental study was carried out to elaborate the physicochemical properties of particles in-flight during the SAPS process. One type of commercially available agglomerated and sintered yttria-stabilized-zirconia (YSZ) powder was injected into the SAPS plasma jet and collected by the shock chilling method. The YSZ particles' in-flight physicochemical properties during the SAPS process, including melting state, morphology, microstructure, particle size distribution, element composition changes, and phase transformation, have been systematically analyzed. The melting state, morphology, and microstructure of the collected particles were determined by scanning electron microscopy (SEM). The particle size distribution was measured by a laser diffraction particle size analyzer (LDPSA). Element compositions were quantitatively analyzed by an electron probe X-ray microanalyzer (EPMA). Additionally, the X-ray diffraction (XRD) method was used to analyze the phase transformation. The results showed that the original YSZ powder injected into the SAPS plasma jet was quickly heated and melted from the outer layer accompanied with breakup and collision-coalescence. The outer layer of the collected particles containing roughly hexagonal shaped grains exhibited a surface texture with high sphericity and the inside was dense with a hollow structure. The median particle size had decreased from 45.65 to 42.04 μm . In addition to this, phase transformation took place, and the content of the zirconium (Zr) and yttrium (Y) elements had decreased with the evaporation of ZrO_2 and Y_2O_3 .

Keywords: plasma spray; in-flight particles; molten status; YSZ

1. Introduction

Thermal barrier coatings (TBCs), which can provide thermal insulation to hot components of engines to protect them from corrosion and oxidation at high temperatures, play an important role in advanced gas-turbine and diesel engines [1–3]. A typical TBCs system consists of two layers over a super alloy substrate: a metallic bond-coat and a ceramic top-coat, where yttria-stabilized-zirconia (Y_2O_3 stabilized ZrO_2 , YSZ) is a widely used material for the top coat owing to its low thermal conductivity, high thermal expansion coefficient, and good mechanical properties [4,5]. To date, electron beam physical vapor deposition (EB-PVD) and atmospheric plasma spraying (APS) are the two main processes to prepare YSZ coatings. In particular, APS is a commercial, high-efficiency, process

and easy to operate, in which raw powder is injected into the plasma jet with a carrier gas and quickly heated and accelerated. Successive particles in-flight impinge onto the substrate followed by spreading and rapid solidification to form single splats. The as-sprayed coating develops with the stacking of these flattened splats [6,7].

At present, empirically tuning 3–6 main controllable parameters is the main method to find the relationship between the spray parameters and the coating [8,9]. However, APS is a complicated process in which more than 35 main parameters, both controllable parameters (such as the flow rate of gas, power, etc.) and some uncontrollable parameters (like the erosion of the electrode, and fluctuations in the particles' injection geometry), are identified to influence the resulting microstructure and corresponding coating properties [10]. Therefore, it is a great challenge to produce reproducible and reliable plasma sprayed coatings. In recent years, particles' in-flight properties have been studied theoretically, numerically, and experimentally and this has suggested that no matter how complicated the influence parameter is, the physicochemical properties of particles in-flight before impinging onto the substrate are fundamental parameters influencing the quality of the as-sprayed coatings [11–16]. Liu et al. [11] used the Box–Behnken Design experimental method to analyze the effect of spray parameters on the average velocity and surface temperature of $\text{La}_2\text{Ce}_2\text{O}_7$ particles in-flight and their influence on microstructure and mechanical properties. Bai et al. [12] adopted the one-factor-at-a-time method to investigate the effect of four spray parameters on the average velocity and temperature of nanostructured YSZ particles in-flight and to theoretically quantify the influence of in-flight particles' melting state on the microstructure of as-sprayed coatings. Choudhury et al. [13] utilized an Artificial Neural Network (ANN) to quantify the relationship between processing parameters and Al_2O_3 - TiO_2 particles' in-flight characteristics, and to establish process controls by predicting the particles' in-flight characteristics in the APS process. Suffner et al. [14] investigated the rapid solidification behavior of the Al_2O_3 , ZrO_2 , and Y_2O_3 molten droplets after impacting on the liquid nitrogen cooled substrate. Wei et al. [15] analyzed the melting state and refining behavior of particles' flight during spraying using a numerical method. Tekmen et al. [16] investigated the oxidation behavior of Al particles in-flight and the effects of velocity and temperature on particles in-flight with an oxidation mechanism.

Lately, an advanced high efficiency and low energy consumption (lower than 80 kW) supersonic atmospheric plasma spraying (SAPS) process has been successfully developed by the Academy of Armored Forces Engineering (Beijing, China) [17,18]. The main components of this novel system are a plasma gun, a powder feeder, a gas-supply system, a cooling water system, and a power supply and control system. Figure 1 shows a schematic diagram of the supersonic plasma spraying system. The key to this system is a novel SAPS gun with a Laval nozzle and internal feedstock injection mode, which means the feedstock particles can be heated and accelerated adequately with no limitation to the melting temperature of the sprayed materials, and it has greater advantage in fabricating high performance ceramic, cermet, or metallic coatings than APS. However, the physicochemical properties of YSZ particles in-flight during the SAPS process have not yet been systematically studied.

Motivated by the aforementioned considerations, this study is dedicated to understanding the physicochemical properties of YSZ particles in-flight by using experimental methods to achieve better knowledge of TBCs using the SAPS process. We note that it is difficult to directly observe the physicochemical properties of YSZ particles in-flight during the SAPS process due to their high temperature and velocity. In this paper, a shock chilling method was employed to trap the YSZ in-flight particles at the usual spraying distance during the SAPS process. The YSZ particles in-flight physicochemical properties including melting state, morphology, microstructure, particle size distribution, element composition changes, and phase transformation were investigated in detail during the SAPS process.

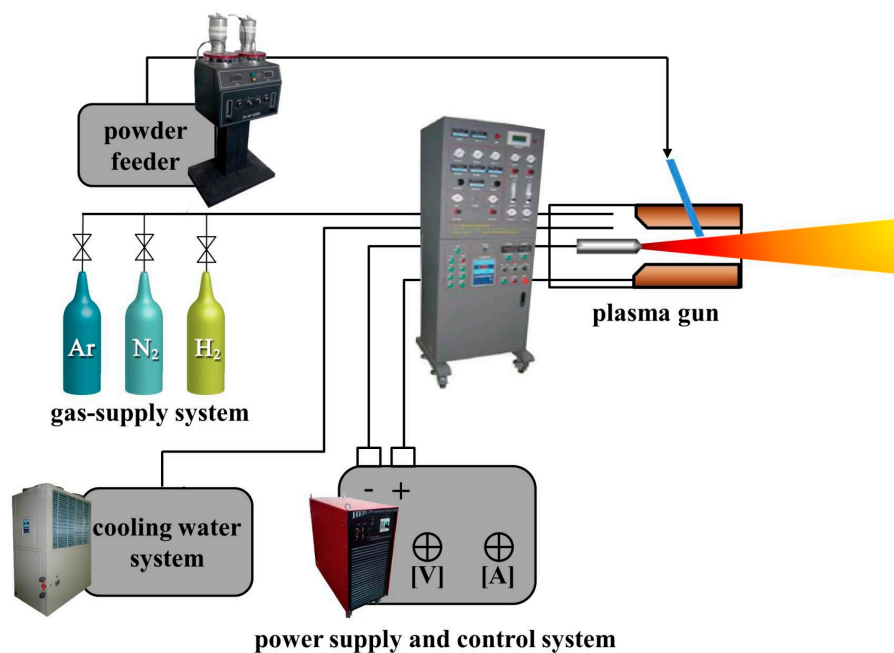


Figure 1. Schematic diagram of the supersonic plasma spraying system.

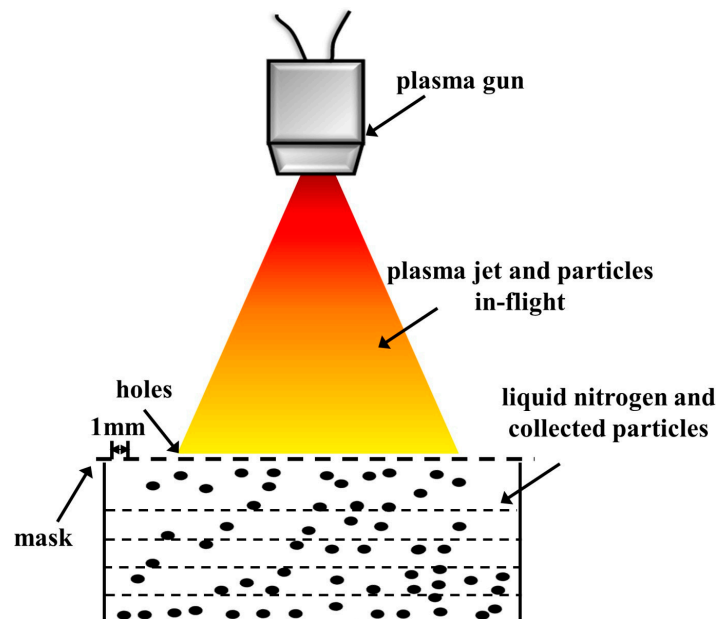
2. Experimental Material and Methods

Experiments were carried out on a SAPS system (HEPJ-II, Beijing, China) and the plasma gun was mounted on a 6-axis robot (MOTOMAN-2010, Ysakawa, Japan). Details of the spraying parameters are listed in Table 1, in which argon and hydrogen were used as the primary and assistant gases, respectively. One type of commercially available agglomerated and sintered (AS) 6–8 wt. % Y_2O_3 - ZrO_2 (YSZ) particles was used as feedstock. To collect particles in-flight before impinging onto the substrate, an experimental apparatus was developed (as illustrated in Figure 2). During the SAPS process, YSZ particles in-flight were rapidly solidified and collected in a collection apparatus containing liquid nitrogen in which the cooling rate of the spraying particles exceeded 10^6 K/s that enabled a rapid cooling rate [19]. Furthermore, liquid nitrogen, an inert cooling medium, was used to prevent chemical reaction from occurring between the YSZ particles in-flight and the cooling medium. Thus, this shock chilling method could be used to characterize the physicochemical properties of YSZ particles in-flight. The collection apparatus was positioned vertically to the SAPS gun to enable the YSZ particles in-flight to fly into the liquid nitrogen. The trapped particles were extracted from the resulting suspension by a membrane filter with a pore diameter of $0.1 \mu m$ and then dried in a vacuum drying box. The external and internal morphology of the original AS YSZ powders (referred as O-AS) and collected YSZ particles (referred as C-AS) were determined by a scanning electron microscope (SEM, GeminiSEM 500, ZEISS, Oberkochen, Germany). The particle size distribution of the O-AS powders and C-AS particles was measured by a laser diffraction particle size analyzer (LDPSA, Horiba LA-950, Kyoto, Japan). Element compositions of the O-AS powders and C-AS particles were quantitatively analyzed by using wavelength dispersive X-ray spectroscopy (WDS) in an electron probe X-ray microanalyzer (EPMA, EMAX-1770, Kyoto, Japan) with a resolution of 110 ppm and operating voltage at 20 kV. In order to determine the element compositions of the original O-AS powders and C-AS particles accurately, five measurement points were randomly obtained in one image during analysis. The final value was calculated using 15 images selected randomly. The phase transformation of the O-AS powders was characterized by X-ray diffraction (XRD, Philips X'Pert Pro, Almelo, Holland) under room temperature with Cu $K\alpha$ radiation of wavelength 1.5418 \AA . The scanning 2θ angle ranged from 10° to 90° with a step scanning rate of $0.02^\circ/\text{min}$, while the voltage and electric current were held at 40 kV and 30 mA, respectively. The samples were determined three times, respectively.

Table 1. Spray parameters of yttria-stabilized-zirconia (YSZ) by supersonic atmospheric plasma spraying (SAPS).

Current (A)	Voltage (V)	Ar Gas (slpm #)	H ₂ Gas (slpm)	Carrier Gas (slpm)	Powder Feeding Rate (g/min)	Spray Distance (mm)	Injector Diameter (mm)	Spraying Angle (°)
430	150	120	24.2	7	35	100	2.2	90

slpm: standard liter per minute.

**Figure 2.** Schematic illustration of particles' in-flight collecting apparatus.

3. Results and Discussion

3.1. Characterization of the O-AS Powders and C-AS Particles

Characteristics of the O-AS powders are shown in Figure 3. The overall surface morphology of the O-AS powders and the high magnification SEM micrograph of a single powder are shown in Figure 3a,b, respectively. It can be seen that the O-AS powders are composed of agglomerated primary granules with 1–2 μm diameter. The O-AS powders with a rough surface are near spherical morphology which can ensure good flow ability. Figure 3c,d reveals the cross-sectional morphology of the O-AS powders, which indicates that the inside of the particles has a relatively loose and porous microstructure. Figures 4 and 5 show the surface and cross-sectional SEM micrographs of the C-AS particles passed through the SAPS plasma jet. Compared with the O-AS powders (Figure 3), the C-AS particles after the SAPS plasma jet exhibited a smoother surface with high sphericity (Figure 4a) due to the surface of the O-AS powders being immediately melted by the high temperature of the SAPS plasma jet when injected into the SAPS plasma jet and the surface of the melted particles becoming spherical under the effect of surface tension [20]. The surface texture of the C-AS particles could be clearly seen when the C-AS particles were more closely examined (see Figure 4b), which may be due to the molten primary granules with 1–2 μm diameter being rapidly cooled and some roughly hexagonal shaped grains being formed. Figure 4c,d displays the cross-sectional morphology of the C-AS particles, which indicates that the C-AS particles with a hollow structure are denser than the O-AS powders with a relatively loose and porous microstructure. This is because the formation of a liquid outer layer prevented further escape of the gas from the O-AS powders and the inside of the particles in-flight continued to melt with the increase of flight distance [21]. As can be seen in

Figure 4, there are many smaller and exploded C-AS particles due to the trapped gas expanding when heated, resulting in an explosion and breakup, which can be attributed to the effect of surface tension, shear force, and pressure inside the particles in-flight. There are also some bigger particles, which may be attributed to the collision and coalescence of the particles in-flight during the SAPS process (see Figure 5a) [22]. Figure 5b shows the molten surface microstructure of the particles in-flight at the initial SAPS process stage.

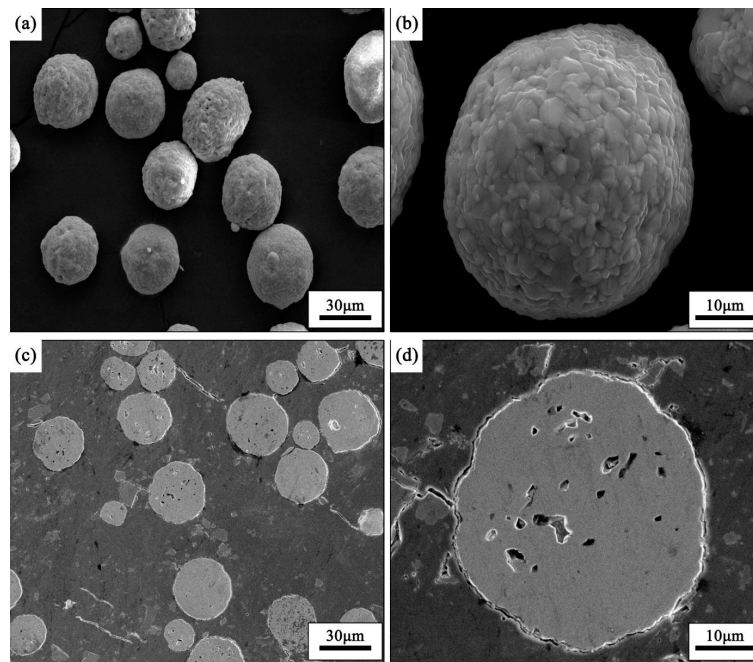


Figure 3. Surface and cross-sectional SEM micrographs of the agglomerated and sintered yttria-stabilized-zirconia (O-AS) powders: (a) overall surface morphology; (b) surface morphology under high magnification; (c) overall cross-sectional morphology; and (d) cross-sectional morphology under high magnification.

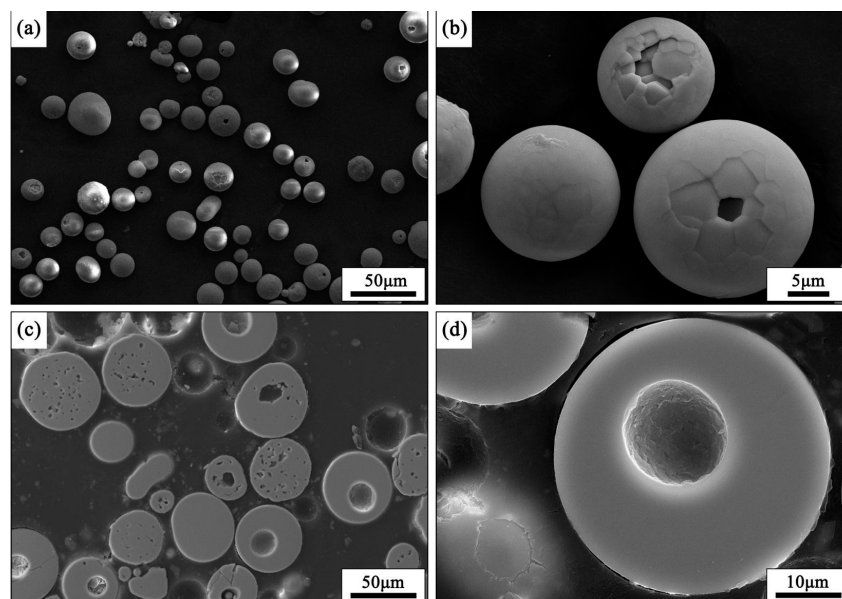


Figure 4. Surface and cross-sectional SEM micrographs of the collected YSZ particles (referred as C-AS) particles: (a) overall surface morphology; (b) surface morphology under high magnification; (c) overall cross-sectional morphology; and (d) cross-sectional morphology under high magnification.

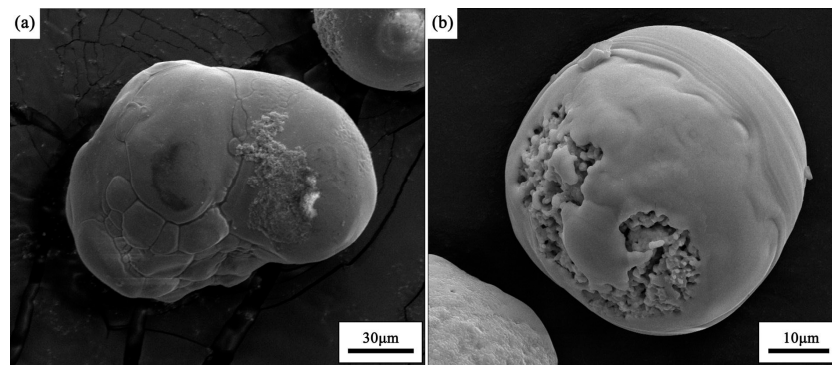


Figure 5. (a) Surface SEM micrographs of collision-coalescence particles during the SAPS process and (b) molten surface microstructure of the particles in-flight at the initial SAPS process stage.

3.2. Particle Size Distribution of the O-AS Powders and C-AS Particles

The particle size distribution of the O-AS powders and C-AS particles is given in Figure 6. The median particle sizes (D_{50}) of the original AS YSZ particles and collected YSZ particles were 45.65 μm and 42.04 μm , respectively. The values of D_{10} , D_{50} , and D_{90} are summarized in Table 2. As can be seen from the result, the particle size of the O-AS powders which were injected into the plasma jet obviously decreased during the SAPS process. The possible causes of the particles' in-flight refining were analyzed as follows: 1) as the particles in-flight melt during the SAPS process, the particles in-flight become smaller and denser; 2) The molten particles in-flight may breakup during the SAPS process that further results in the reduced particle size. The smaller particles in-flight are able to form coatings with more complex maze structures which is beneficial for thermal insulation and anti-oxidation [23].

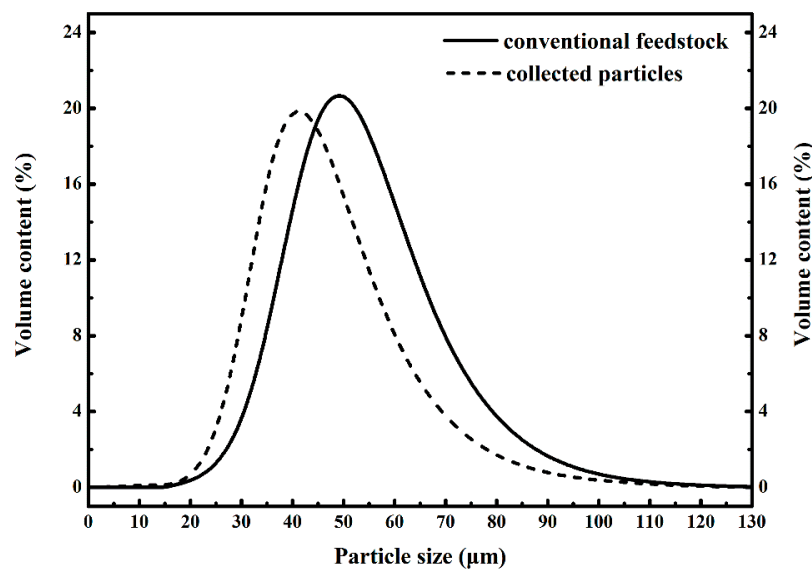


Figure 6. Particle size distribution of the O-AS powders and C-AS particles.

Table 2. Particle size distribution of the O-AS powders and C-AS particles.

State of the YSZ Particles	Particle Size (μm)		
	D_{10}	D_{50}	D_{90}
O-AS powders	32.22	45.65	63.86
C-AS particles	30.16	42.04	60.34

3.3. Element Composition Changes of the O-AS Powders

Element composition of the O-AS powders and C-AS particles measured by EPMA are shown in Figure 7. It can be seen in Figure 7 that the element composition of the O-AS powders and C-AS particles were the same. However, the content of zirconium (Zr, ~65.17 wt. %) and yttrium (Y, ~7.07 wt. %) in the O-AS powders' particles was higher than the C-AS particles (Zr, ~63.58 wt. %; Y, ~4.29 wt. %), while the content of the oxygen element in the O-AS powders was lower. This was probably related to the partial evaporation of ZrO_2 and Y_2O_3 from the original AS YSZ particles during the SAPS process. When the O-AS powders were injected into the plasma jet, in which the temperature was about 10^4 K and much higher than the boiling point of ZrO_2 (~4300 K) and Y_2O_3 (~4300 K), the evaporation of ZrO_2 and Y_2O_3 occurred [24]. As a result, the content of Zr and Y elements decreased. Furthermore, the decrease of Y (~2.78 wt. %) was higher than Zr (~1.59 wt. %), which was ascribed to a higher vapor pressure of Y_2O_3 than ZrO_2 at the elevated temperature (see Figure 8) leading to a faster loss of Y_2O_3 than ZrO_2 during the SAPS process [25].

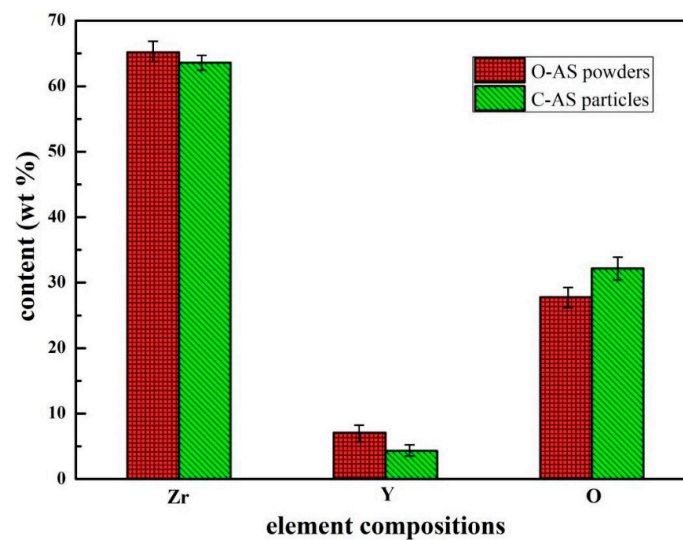


Figure 7. Element compositions of the O-AS powders and C-AS particles.

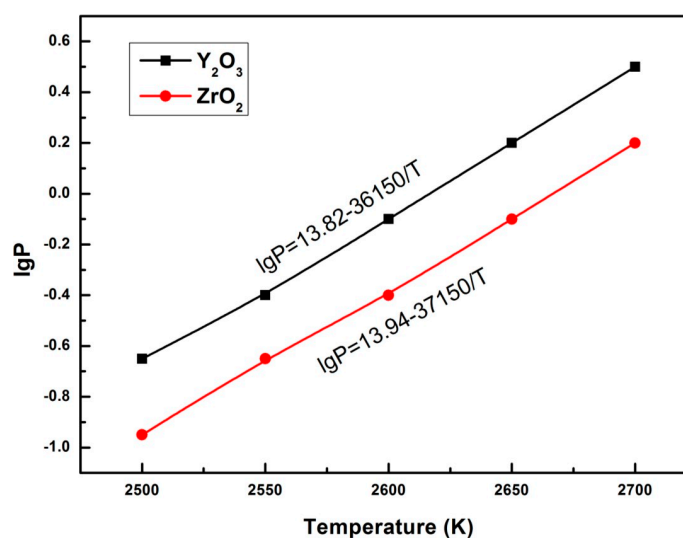


Figure 8. Relationship between temperature and vapor pressure of Y_2O_3 and ZrO_2 .

3.4. Phase Transformation of the O-AS Powders

Figure 9 shows the XRD patterns of the O-AS powders and C-AS particles. According to the XRD patterns shown in Figure 9a, $Y_{0.15}Zr_{0.85}O_{1.93}$, monoclinic zirconia (m- ZrO_2), and Cubic Zirconia (c- ZrO_2) were the main phases of the O-AS powders. It can be seen from Figure 9b that the C-AS particles were mainly composed of $Y_{0.15}Zr_{0.85}O_{1.93}$ and c- ZrO_2 phases. The disappearance of the m- ZrO_2 phase in the O-AS powders during the SAPS process was attributed to phase transformation. As the O-AS powders were passed through the high temperature plasma jet, m- ZrO_2 in the O-AS powders changed into t- ZrO_2 over 1443 K, and then t- ZrO_2 transformed into c- ZrO_2 above 2643 K [26]. The phase transformation of pure ZrO_2 is reversible. However, with the addition of Y_2O_3 stabilizing oxides in the crystalline of ZrO_2 combined with relatively high cooling rates, the amount of phase transformation crystalline ZrO_2 can undergo is limited during the SAPS process. Pure ZrO_2 experiences the following phase transformation:

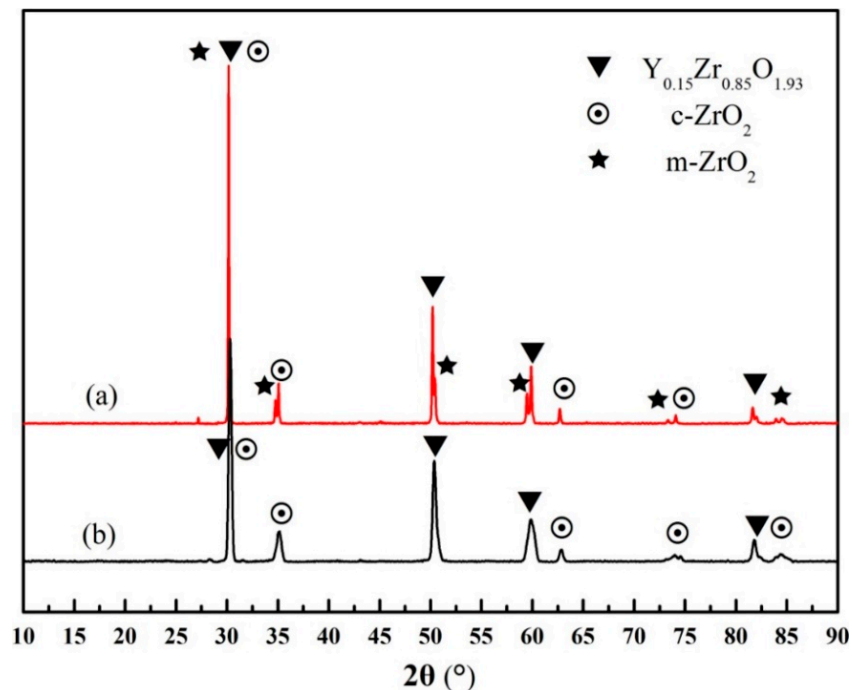
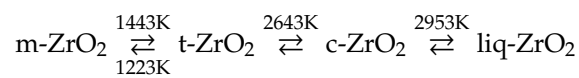


Figure 9. XRD patterns of (a) the O-AS powders and (b) C-AS particles.

Figure 10 shows the surface and cross-sectional morphologies of C-AS particles. It can be observed that larger pores appear inside and on the surface of spraying particles compared with O-AS particles given in Figure 3. A schematic diagram representing the development of physicochemical properties of YSZ particles in-flight during supersonic atmospheric plasma spray is shown in Figure 11. The physicochemical properties of YSZ particles in-flight before impinging onto the substrate can significantly influence the microstructure and phase composition of the as-sprayed coatings. The relationship between the physicochemical properties of particles in-flight and the properties of high efficiency supersonic atmospheric plasma-sprayed YSZ coatings still need to be investigated.

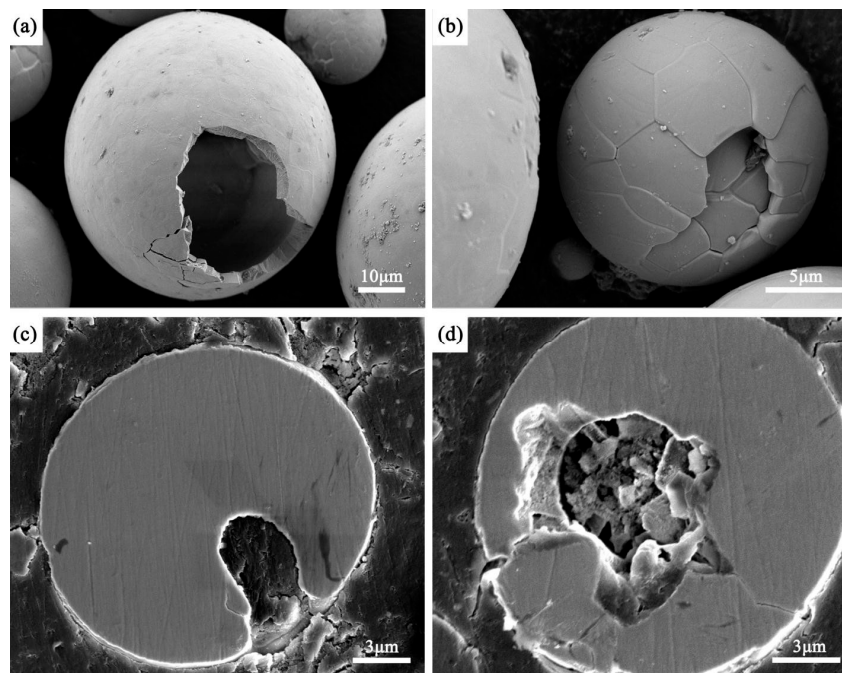


Figure 10. Morphologies of C-AS particles: (a,b) surface morphologies; (c,d) cross-sectional morphologies.

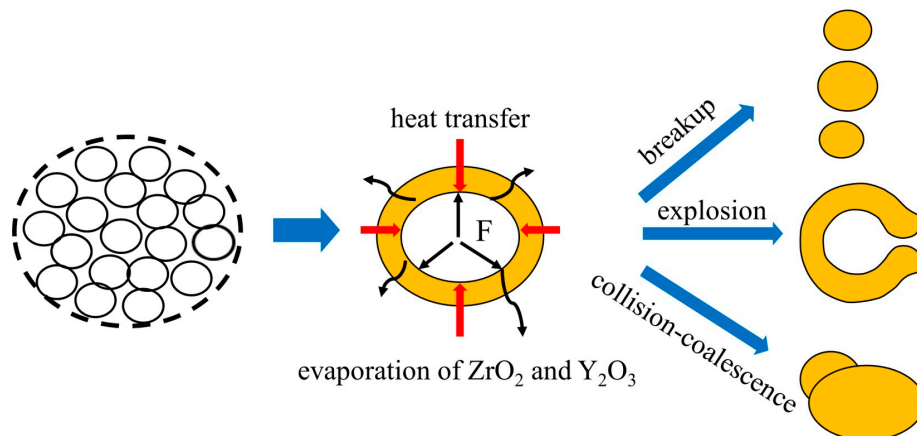


Figure 11. Schematic diagram of the development of physicochemical properties of YSZ particles in-flight during the SAPS process.

4. Conclusions

In this study, YSZ particles in-flight were successfully collected by a shock chilling method using a collection apparatus containing liquid nitrogen, and the physicochemical properties of the melting state, morphology, microstructure, particle size, chemical composition changes, and phase transformation during the SAPS process have been systematically investigated and the following conclusions can be drawn:

- (1) The O-AS powder injected into the SAPS plasma jet was quickly heated and melted from the outer layer accompanied with breakup and collision-coalescence. The outer layer of the C-AS particles containing roughly hexagonal shaped grains exhibited a surface texture with high sphericity and the inside was dense with a hollow structure.

- (2) The molten YSZ particles in-flight became smaller and denser and may have broken up during the SAPS process. As a result, there was a refining phenomenon of particles in-flight during the SAPS process. The median particle size decreased from 45.65 to 42.04 μm .
- (3) The element composition of the O-AS powder and C-AS particles were the same. However, the content of Zr and Y (wt. %) in the O-AS powder particles was higher than the C-AS particles. The content of Zr and Y (wt. %) decreased with the evaporation of ZrO_2 and Y_2O_3 during the SAPS process, respectively. Furthermore, the decrease of Y (~2.78 wt. %) was higher than Zr (~1.59 wt. %).
- (4) Phase transformation took place during the SAPS process. The O-AS powders were mainly composed of $\text{Y}_{0.15}\text{Zr}_{0.85}\text{O}_{1.93}$, m- ZrO_2 , and c- ZrO_2 phases; the corresponding C-AS particles were mainly composed of $\text{Y}_{0.15}\text{Zr}_{0.85}\text{O}_{1.93}$ and c- ZrO_2 phases. The m- ZrO_2 phase vanished during the SAPS process.

Author Contributions: G.M. wrote the paper; S.C. analyzed the data; J.K. designed the experiments; H.W. and G.L. performed the experiments; M.L. conduct literature search; Q.Z. contributed to the figures and tables; P.H. polished the grammar of the paper.

Funding: This research was funded by the National Nature Science Foundation of China (51675531, 51535011, and 51675158), the Beijing Municipal Natural Science Foundation (3172038), Joint Fund of Ministry of Education for Pre-research of Equipment for Young Personnel Project (6141A02033120) and the Tribology Science Fund of State Key Laboratory of Tribology (SKLTKF16A05).

Conflicts of Interest: The authors declare no conflict of interest. The research was funded by National Nature Science Foundation of China, Nature Science Foundation of Beijing and The Tribology Science Fund of State Key Laboratory of Tribology. The founding sponsors had no role in the design of the study; in the collection, analyses, or interpretation of data; in the writing of the manuscript, and in the decision to publish the results.

References

1. Wang, C.; Wu, T. TiO_2 nanoparticles with efficient photocatalytic activity towards gaseous benzene degradation. *Ceram. Int.* **2015**, *41*, 2836–2839. [[CrossRef](#)]
2. Evans, A.G.; Clarke, D.R.; Levi, C.G. The influence of oxides on the performance of advanced gas turbines. *J. Eur. Ceram. Soc.* **2008**, *28*, 1405–1419. [[CrossRef](#)]
3. Kitazawa, R.; Tanaka, M.; Kagawa, Y.; Liu, Y.F. Damage evolution of TBC system under in-phase thermo-mechanical tests. *Mater. Sci. Eng. B Adv.* **2010**, *173*, 130–134. [[CrossRef](#)]
4. Clarke, D.R.; Phillpot, S.R. Thermal barrier coating materials. *Mater. Today* **2005**, *8*, 22–29. [[CrossRef](#)]
5. Dong, H.; Yang, G.J.; Cai, H.N.; Ding, H.; Li, C.X.; Li, C.J. The influence of temperature gradient across YSZ on thermal cyclic lifetime of plasma-sprayed thermal barrier coatings. *Ceram. Int.* **2015**, *41*, 11046–11056. [[CrossRef](#)]
6. Padture, N.P.; Gell, M.; Jordan, E.H. Thermal barrier coatings for gas-turbine engine applications. *Science* **2002**, *296*, 280–284. [[CrossRef](#)] [[PubMed](#)]
7. Vijay, K.; Balasubramanian, K. Processing and design methodologies for advanced and novel thermal barrier coatings for engineering applications. *Particuology* **2016**, *27*, 1–28.
8. Fauchais, P.; Vardelle, M.; Goutier, S. Latest researches advances of plasma spraying: From splat to coating formation. *J. Therm. Spray Technol.* **2016**, *25*, 1534–1553. [[CrossRef](#)]
9. Bai, Y.; Zhao, L.; Tang, J.J.; Ma, S.Q.; Ding, C.H.; Yang, J.F.; Yu, L.; Han, Z.H. Influence of original powders on the microstructure and properties of thermal barrier coatings deposited by supersonic atmospheric plasma spraying, part II: Properties. *Ceram. Int.* **2013**, *39*, 4437–4448. [[CrossRef](#)]
10. Vardelle, A.; Vardelle, M.; Fauchais, P. Influence of velocity and surface temperature of alumina particles on the properties of plasma sprayed coatings. *Plasma Chem. Plasma Process.* **1982**, *2*, 255–291. [[CrossRef](#)]
11. Liu, K.; Tang, J.; Bai, Y.; Yang, Q.; Wang, Y.; Kang, Y.; Zhao, L.; Zhang, P.; Han, Z. Particle in-flight behavior and its influence on the microstructure and mechanical property of plasma sprayed $\text{La}_2\text{Ce}_2\text{O}_7$ thermal barrier coatings. *Mater. Sci. Eng. A* **2015**, *625*, 177–185. [[CrossRef](#)]
12. Bai, Y.; Zhao, L.; Qu, Y.M.; Fu, Q.Q.; Wang, Y.; Liu, K.; Tang, J.J.; Li, B.Q.; Han, Z.H. Particle in-flight behavior and its influence on the microstructure and properties of supersonic-atmospheric-plasma-sprayed nanostructured thermal barrier coatings. *J. Alloy. Compd.* **2015**, *644*, 873–882. [[CrossRef](#)]

13. Choudhury, T.A.; Hosseinzadeh, N.; Berndt, C.C. Artificial Neural Network application for predicting in-flight particle characteristics of an atmospheric plasma spray process. *Surf. Coat. Technol.* **2011**, *205*, 4886–4895. [[CrossRef](#)]
14. Suffner, J.; Lattemann, M.; Hahn, H.; Giebeler, L.; Hess, C.; Cano, I.G.; Dosta, S.; Guilemany, J.M.; Musa, C.; Locci, A.M.; et al. Microstructure Evolution During Spark Plasma Sintering of Metastable (ZrO₂-3 mol % Y₂O₃)-20 wt % Al₂O₃ Composite Powders. *J. Am. Ceram. Soc.* **2010**, *9*, 2864–2870. [[CrossRef](#)]
15. Wei, P.; Wei, Z.; Zhao, G.; Du, J.; Bai, Y. The analysis of melting and refining process for in-flight particles in supersonic plasma spraying. *Comput. Mater. Sci.* **2015**, *103*, 8–19.
16. Tekmen, C.; Tsunekawa, Y.; Yoshida, M.; Okumiya, M. Microstructural Characterization of In-flight Particles in Plasma Spray Process. *Plasma Process. Polym.* **2009**, *6*, S223–S226. [[CrossRef](#)]
17. Zhang, X.C.; Xu, B.S.; Wu, Y.X.; Xuan, F.Z.; Tu, S.T. Porosity, mechanical properties, residual stresses of supersonic plasma-sprayed Ni-based alloy coatings prepared at different powder feed rates. *Appl. Surf. Sci.* **2008**, *254*, 3879–3889. [[CrossRef](#)]
18. Bai, Y.; Zhao, L.; Liu, K.; Tang, J.J.; Han, Z.H. Fine-lamellar structured thermal barrier coatings fabricated by high efficiency supersonic atmospheric plasma spraying. *Vacuum* **2014**, *99*, 119–123. [[CrossRef](#)]
19. Yan, J.H.; Xu, J.J.; Wang, Y.; Liu, L.F. Preparation of agglomerated powders for air plasma spraying MoSi₂ coating. *Ceram. Int.* **2015**, *41*, 10547–10556. [[CrossRef](#)]
20. Vassen, R.; Schwartz, S.; Jungen, W. Spray-drying of ceramics for plasma-spray coating. *J. Eur. Ceram. Soc.* **2000**, *20*, 2433–2439.
21. Pravdic, G.; Gani, M.S.J. The formation of hollow spherical ceramic oxide particles in a d.c. plasma. *J. Mater. Sci.* **1996**, *31*, 3487–3495. [[CrossRef](#)]
22. Lehtinen, K.E.J.; Zachariah, M.R. Energy accumulation in nanoparticle collision and coalescence processes. *J. Aerosol Sci.* **2002**, *33*, 357–368. [[CrossRef](#)]
23. Wang, C.; Li, K.; Shi, X.; Huo, C.; He, Q.; Zhang, Y. Effect of spraying power on oxidation resistance and mechanical properties of plasma sprayed La-Mo-Si coating. *Surf. Coat. Technol.* **2017**, *311*, 138–150. [[CrossRef](#)]
24. Garvie, R.C.; Hannink; Amp, R.H.; Pascoe, R.T. Ceramic steel. *Nature* **1975**, *258*, 703–704. [[CrossRef](#)]
25. Zhao, L.; Bai, Y.; Tang, J.J.; Liu, K.; Ding, C.H.; Yang, J.F.; Han, Z.H. Effect of particle in-flight behavior on the composition of thermal barrier coatings. *Appl. Surf. Sci.* **2013**, *286*, 184–191. [[CrossRef](#)]
26. Lin, G.Y.; Lei, T.C.; Zhou, Y. In-situ TEM observations of tetragonal to monoclinic phase transformation in ZrO₂-2 mol % Y₂O₃ ceramics. *Ceram. Int.* **1998**, *24*, 307–312. [[CrossRef](#)]



© 2019 by the authors. Licensee MDPI, Basel, Switzerland. This article is an open access article distributed under the terms and conditions of the Creative Commons Attribution (CC BY) license (<http://creativecommons.org/licenses/by/4.0/>).